Electronic Supporting Information for:

Does *Z′* Equal 1 or 2? Enhanced Powder NMR Crystallography Verification of a Disordered Room Temperature Crystal Structure of a p38 Inhibitor for Chronic Obstructive Pulmonary Disease

Cory M. Widdifield[a]†, Sten O. Nilsson Lill[b], Anders Broo[b], Maria Lindkvist[b], Anna Pettersen[b], Anna Svensk Ankarberg[b], Peter Aldred[b], Staffan Schantz*[b] and Lyndon Emsley*[c]

[a] Institut des Sciences Analytiques (CNRS/ENS de Lyon/UCB Lyon 1), Centre de RMN à Très Hauts Champs, Université de Lyon, 69100 Villeurbanne, France
[b] AstraZeneca Gothenburg, R&D, Pharmaceutical Technology & Development, SE-431 83 Mölndal, Sweden
[c] Institut des Sciences et Ingénierie Chimiques, Ecole Polytechnique Fédérale de Lausanne (EPFL), CH-1015 Lausanne, Switzerland
† Present address: Department of Chemistry, Durham University, DH1 3LE Durham, United Kingdom

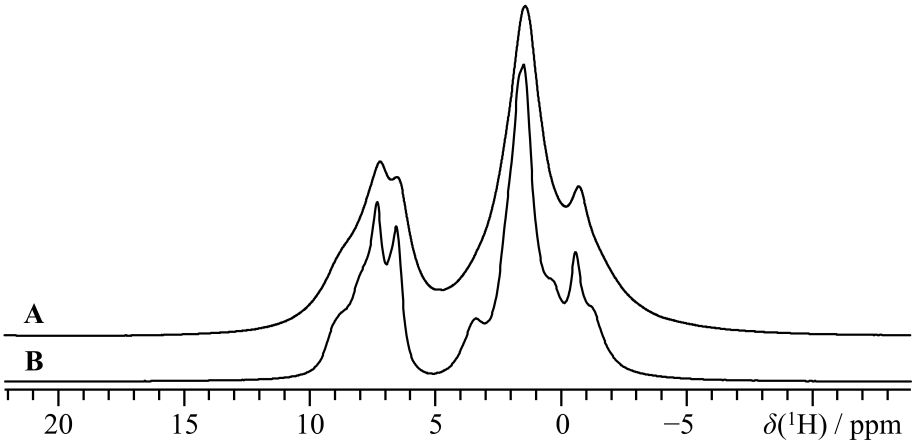

Figure S1. Comparison of ^{1}H echo MAS NMR spectra of **1**, acquired under different conditions. In (**A**), B_0 = 16.4 T and ν_{MAS} = 20.00 kHz (16 scans with a recycle delay of 11.8 s), while in (**B**), B_0 = 11.75 T and ν_{MAS} = 60.94 kHz (*n.b.*, the spectrum in Figure 2 of the main manuscript).

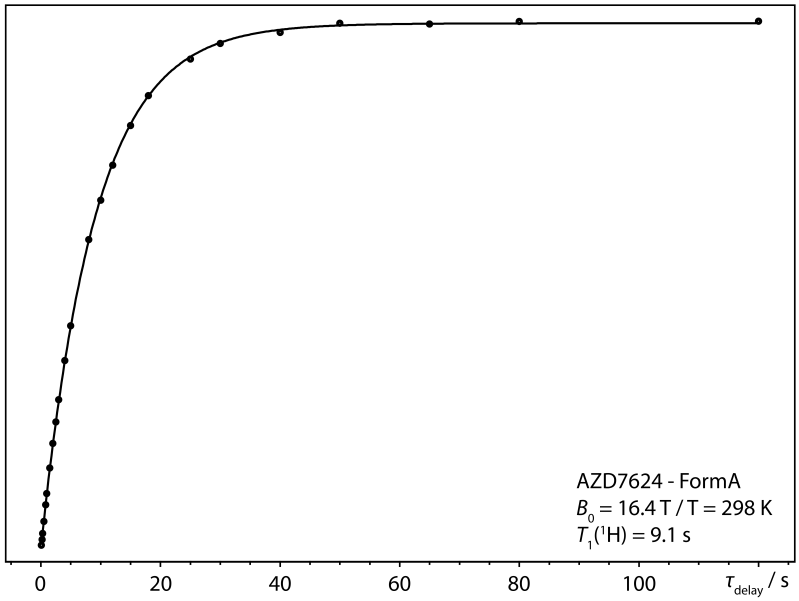

Figure S2. T_1(^{1}H) build-up curve for **1**, measured at B_0 = 16.4 T, T = 298 K, and ν_{MAS} = 20.00 kHz using a saturation recovery pulse sequence with 20 saturating pulses. The time between the saturating pulse loop and the $\pi/2$ read out pulse is given by the horizontal axis, while the vertical axis is the ^{1}H signal intensity, in arbitrary units. For each point, 2 transients were collected and averaged.

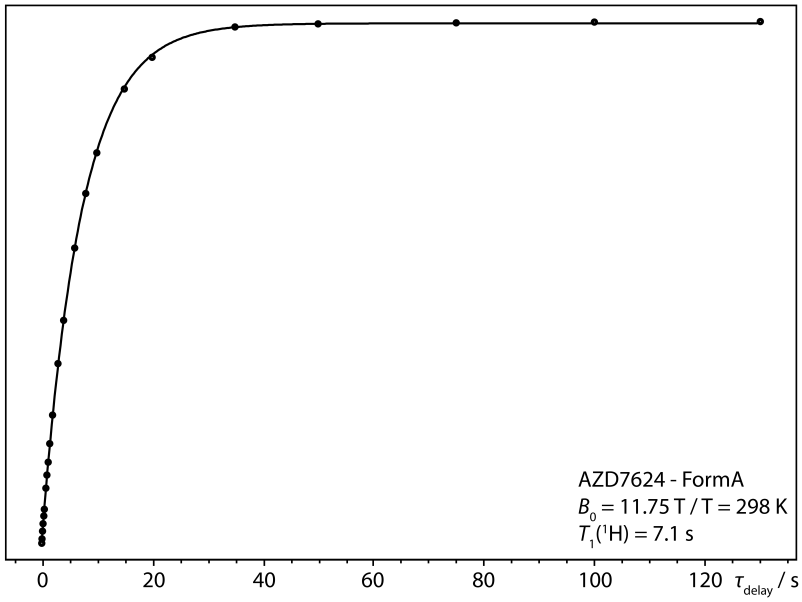

Figure S3. T_1(^{1}H) build-up curve for **1**, measured at B_0 = 11.75 T, T = 298 K, and ν_{MAS} = 12.50 kHz using a saturation recovery pulse sequence with 20 saturating pulses. For each point, 8 transients were collected and averaged.

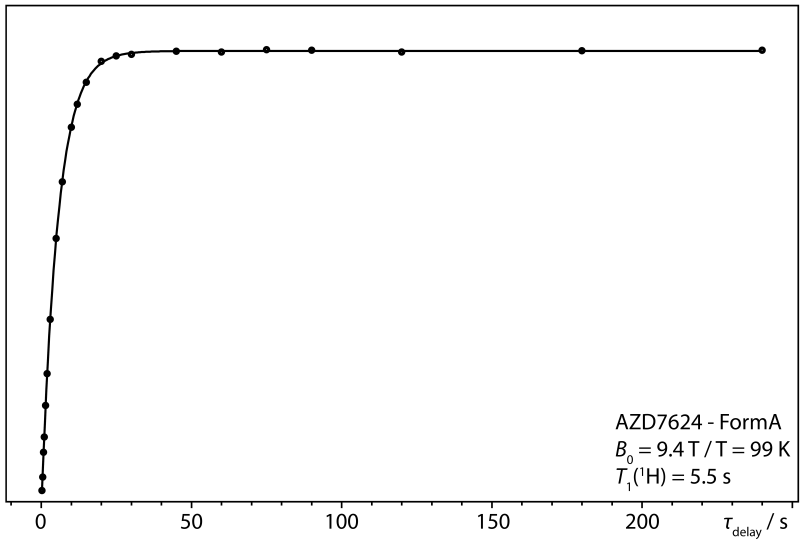

Figure S4. T_1(^{1}H) build-up curve for **1**, measured at B_0 = 9.4 T, T = 99 K, and ν_{MAS} = 10.00 kHz using a saturation recovery pulse sequence with 20 saturating pulses. For each point, 16 transients were collected and averaged.

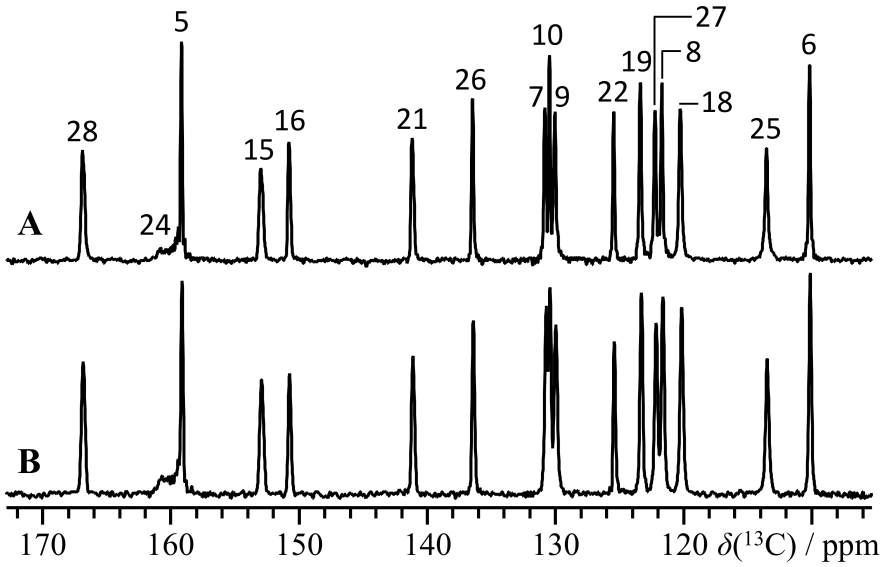

Figure S5. High chemical shift regions of ^{13}C CP/MAS NMR spectra acquired at B_0 = 16.4 T, T = 298 K, and with ν_{MAS} = 12.50 kHz (**A**), and 16.00 kHz (**B**) for **1**. The recycle delay used was 11.8 s for both spectra, with 512 and 760 transients collected and averaged for (**A**) and (**B**), respectively.

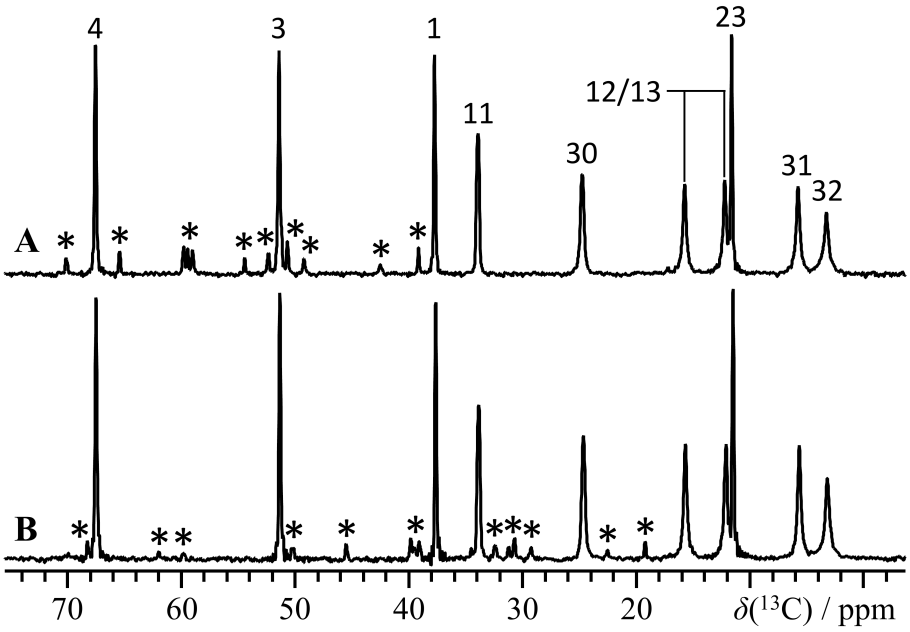

Figure S6. Low chemical shift regions of ^{13}C CP/MAS NMR spectra acquired at B_0 = 16.4 T, T = 298 K, and with ν_{MAS} = 12.50 kHz (**A**), and 16.00 kHz (**B**) for **1**, as in Figure S5. Asterisks denote spinning sidebands and do not correspond to unique chemical sites.

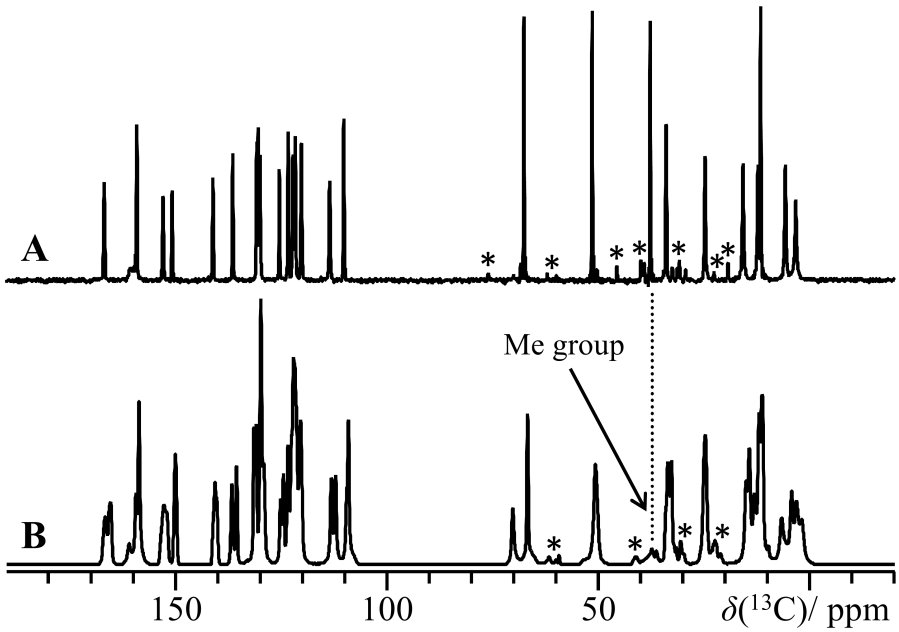

Figure S7. ^{13}C CP/MAS NMR spectra of **1**, acquired at B_0 = 16.4 T, ν_{MAS} = 16.00 kHz and T = 298 K (**A**), and at B_0 = 9.4 T, ν_{MAS} = 10.00 kHz and T = 94 K (**B**). It is clear that there are a significant number of new peaks (nearly double) present in the lower-temperature spectrum. As eventually concluded in the main text, these observations are consistent with dynamic disorder which occurs at the higher temperature being suppressed at the lower temperature (or occurring on a timescale which is much less than the NMR frequency of the spectrum in (**B**), which is ca. 100 MHz). Asterisks denote spinning sidebands. In (**B**), the recycle delay was 10.0 s, with 4752 transients collected and averaged, while (**A**) is the same spectrum depicted in Figures S5**B** and S6**B**. By performing the low-temperature experiment, we also gain clear insight into the identity of the methyl group carbons (as indicated), as this temperature regime is often where methyl group reorientations are transitioning between isotropic and non-isotropic modes.

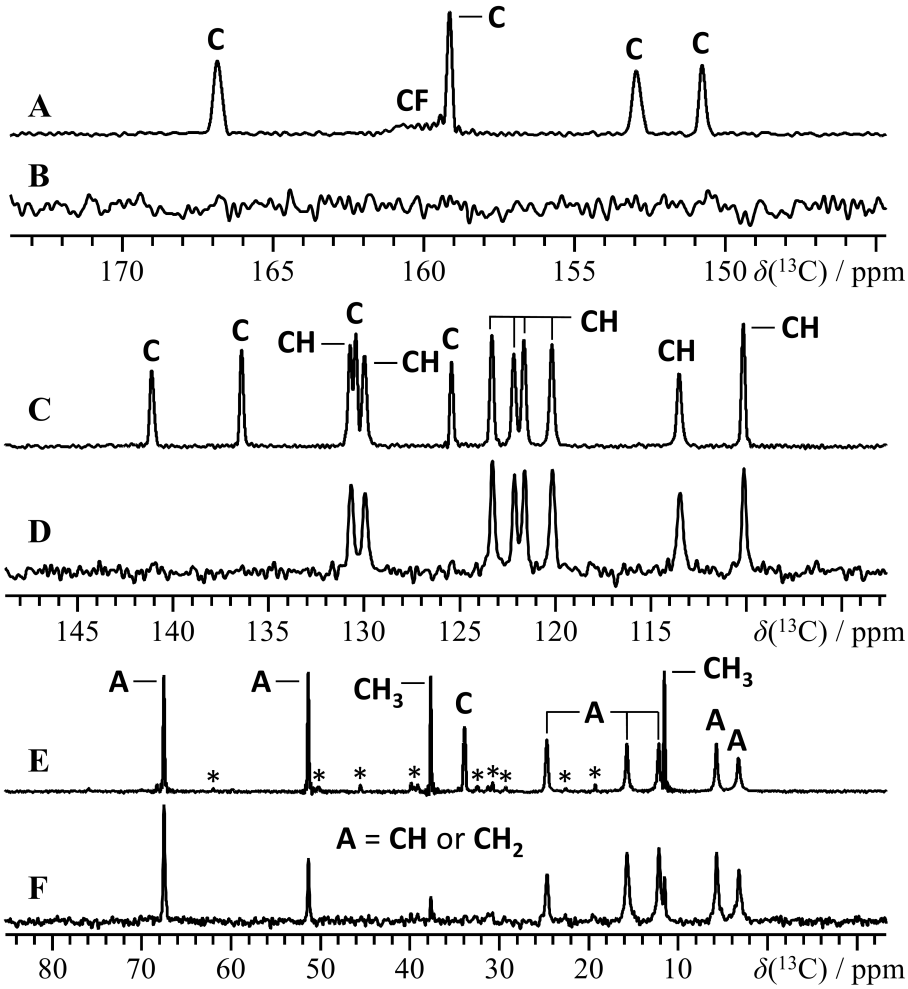

Figure S8. ^{13}C CP/MAS NMR spectra of **1**, acquired at B_0 = 16.4 T with ν_{MAS} = 16.00 kHz and T = 298 K. The spectra in (**A**,**C**,**E**) are collected after a typical CP contact period (2 ms), while the spectra in (**B**,**D**,**F**) are collected using a short CP (SCP) pulse sequence (0.5 ms ^{1}H spin lock followed by a 40 μs contact time). (**A**,**C**,**E**) resulted from 760 transients, while (**B**,**D**,**F**) resulted from 256 transients. For all, the recycle delay was 11.8 s. Asterisks denote spinning sidebands due to MAS. Unambiguous group assignments based only on SCP NMR data are indicated.

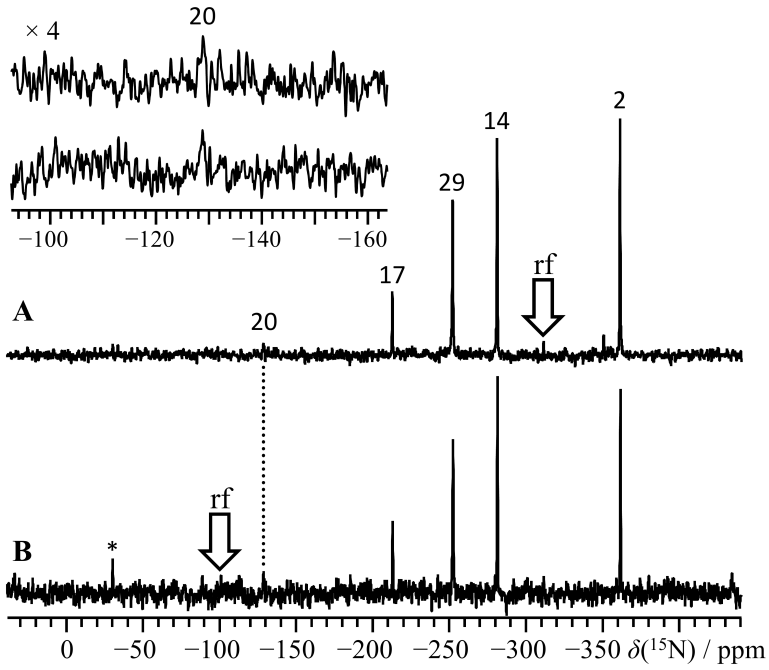

Figure S9. ^{15}N CP/MAS NMR spectra of **1**, acquired at B_0 = 16.4 T with ν_{MAS} = 7.00 kHz and T = 298 K. Spectra in (**A**) and (**B**) were acquired under very similar experimental conditions, except for a change in the radiofrequency (rf) irradiation position, as indicated in each spectrum using an arrow. This was done to excite a portion of the frequency range that would be difficult to excite otherwise. The weak signal from site 20 is tentatively observed, but to clarify, inset above **A** is a horizontal and vertical expansion of the respective spectra for the region near the suspected peak. The asterisk denotes a spinning sideband associated with this site. The spectrum in (**A**) resulted from averaging 5184 transients, while (**B**) resulted from averaging 1112 transients.

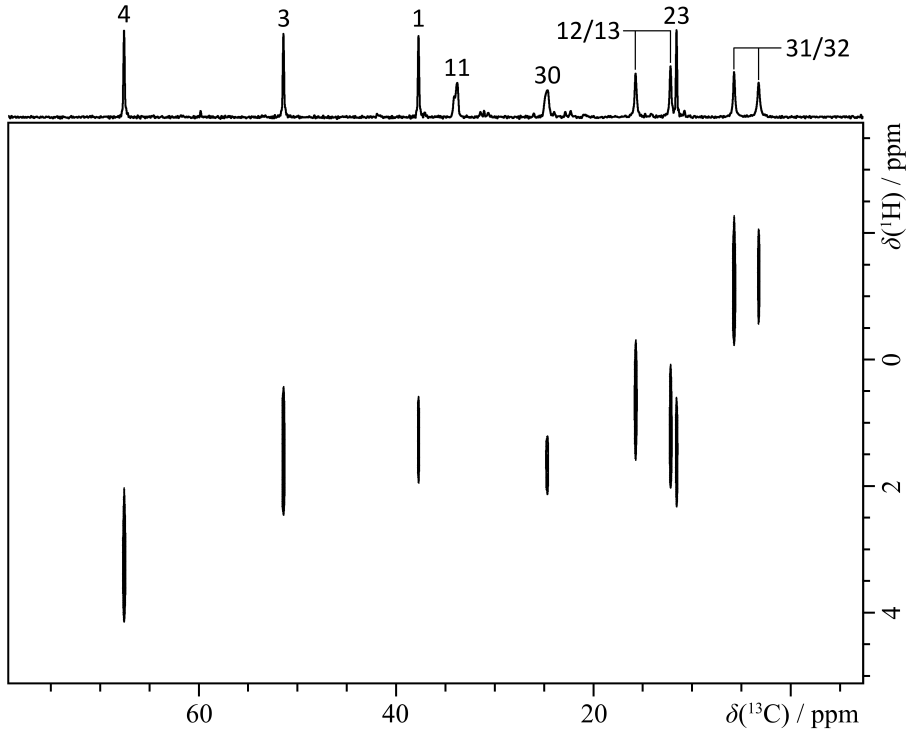

Figure S10. Low-frequency region of the ^{1}H-^{13}C HETCOR NMR spectrum acquired of **1** at B_0 = 11.75 T, T = 293 K and ν_{MAS} = 12.50 kHz. All else is as in Figure 4a of the main paper.

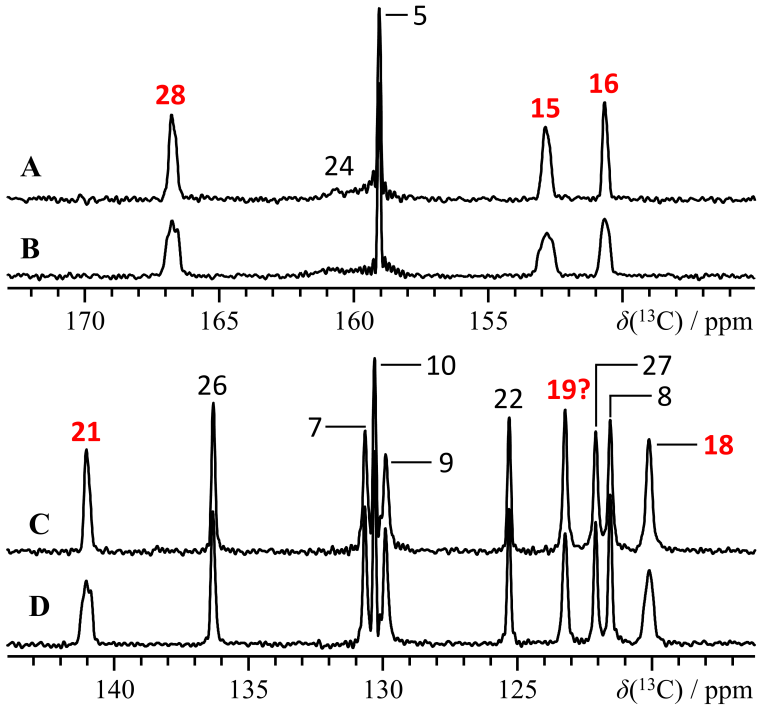

Figure S11. Selected spectral regions of the ^{13}C CP/MAS NMR spectra of **1**, under ν_{MAS} = 12.50 kHz at B_0 = 16.4 T (**A**,**C**) and at B_0 = 11.75 T (**B**,**D**) highlight the residual dipolar coupling between ^{13}C and ^{14}N under MAS. Bold red site labels indicate signals which are consistent with coupling to ^{14}N. One site is suspected of coupling to ^{14}N, but it is not unambiguous (denoted with '?'). A similar process was applied for the other ^{13}C resonances (not shown).

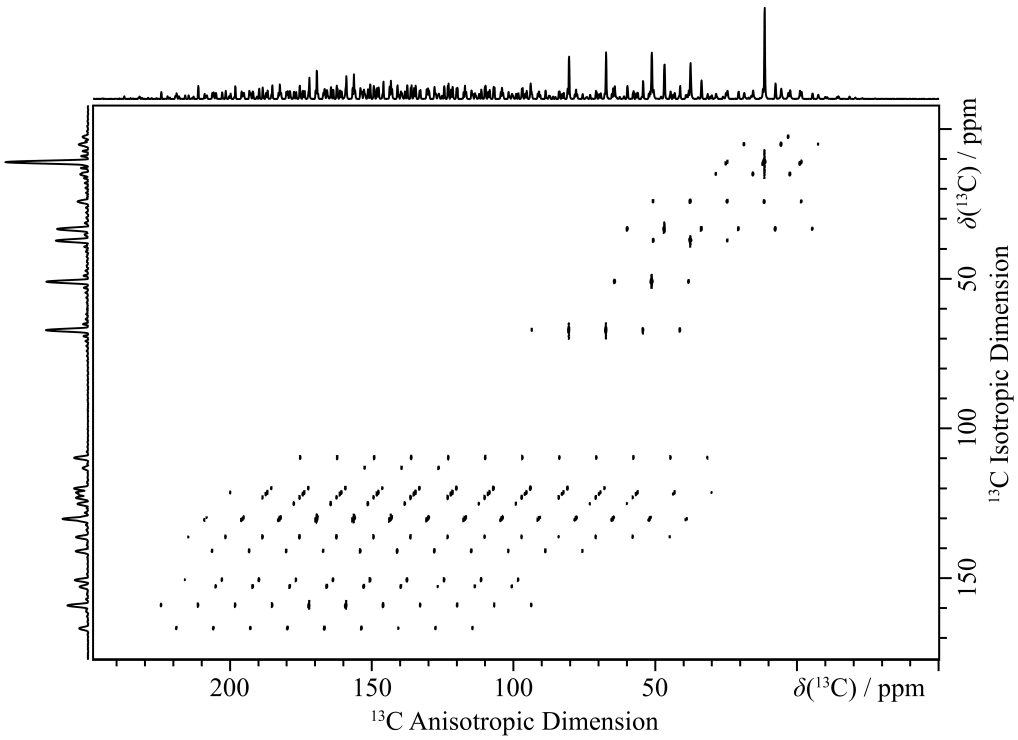

Figure S12. Full ^{13}C-^{13}C 5π-PULSE MAT NMR spectrum of **1** acquired at B_0 = 16.4 T, ν_{MAS} = 2.3 kHz and T = 298 K. The spectrum was acquired with a recycle delay of 11.8 s, 56 transients per t_1 increment, and 256 t_1 increments for a total experiment time of 47 h.

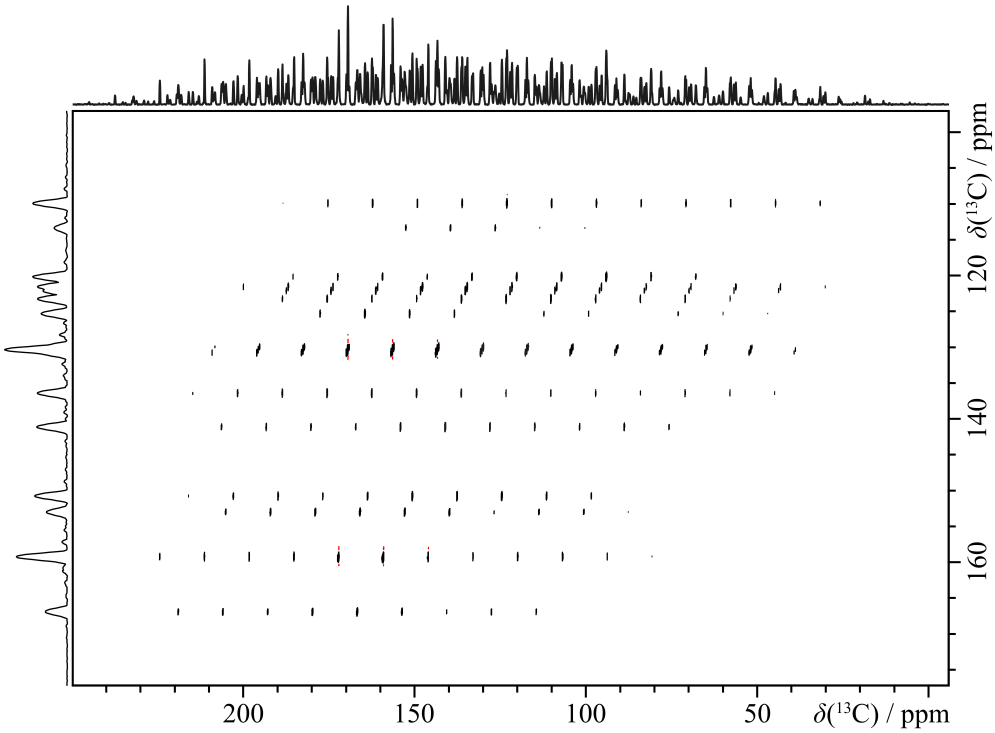

Figure S13. Partial ^{13}C-^{13}C 5π-PULSE MAT NMR spectrum of **1** acquired at B_0 = 16.4 T, ν_{MAS} = 2.3 kHz and T = 298 K, in order to display more spectral detail. This Figure is simply a portion of what was displayed in Figure S12, and otherwise remains as presented in Figure S12.

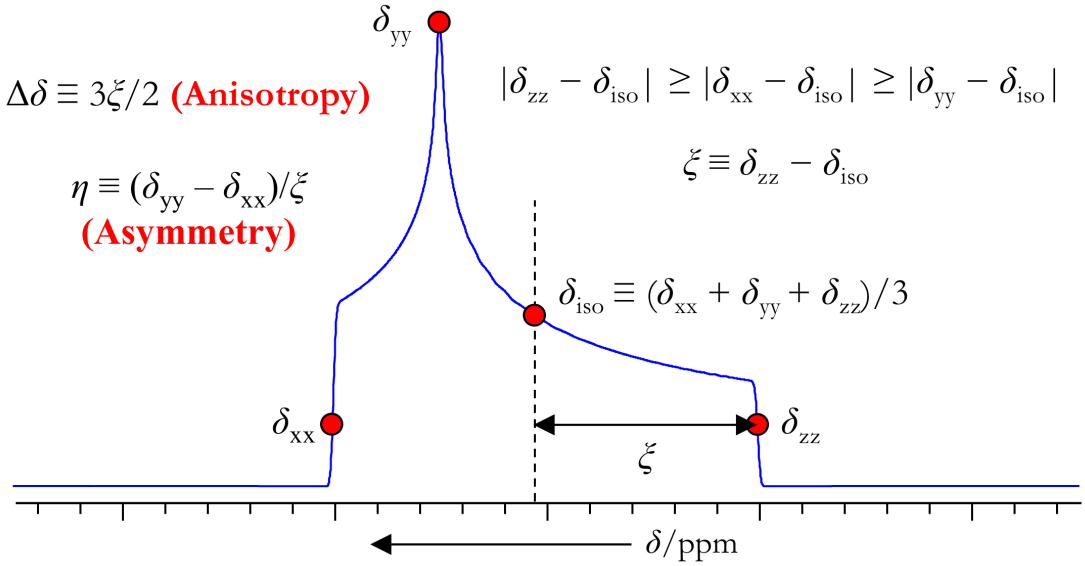

Figure S14. Typical response for an isolated spin-1/2 nucleus in a powdered sample under static conditions (blue trace). The shift tensor parameter definitions are according to the convention of Haeberlen, Mehring, and Spiess.[1-3] The characteristic break points denoted correspond intimately to the anisotropy and asymmetry tensor parameters, as specified.

Table S1. Measured ^{13}C shift tensor parameters for **1**[a]

^{13}C label	δ_{iso} / ppm	$\Delta\delta$ / ppm	η
28	166.85	–116.6(0.6)	0.92(0.01)
24	ca. 160.2	n.d.	n.d.
5	159.13	–123.8(1.4)	0.88(0.02)
15	152.93	–125.7(0.9)	0.76(0.01)
16	150.74	109.1(0.8)	0.75(0.01)
21	141.12	129.8(1.0)	0.91(0.01)
26	136.41	–164.0(0.8)	0.53(0.01)
7	130.74	–172.0(1.5)	0.70(0.02)
10	130.41	–150.7(0.7)	0.35(0.01)
9	129.98	–157.4(1.2)	0.78(0.02)
22	125.39	–156.2(1.1)	0.29(0.01)
19	123.30	131.9(1.4)	0.83(0.01)
27	122.15	–153.6(0.7)	0.64(0.01)
8	121.62	–161.7(1.2)	0.77(0.01)
18	120.17	124.3(0.9)	0.53(0.01)
25	113.46	–143.4(1.5)	0.47(0.02)
6	110.10	–146.9(0.8)	0.70(0.01)
4	67.52	–52.1(0.3)	< 0.01
3	51.35	–33.8(0.3)	0.46(0.02)
1	37.65	–32.2(0.2)	< 0.01
11	33.84	–74.2(0.8)	0.15(0.02)
30	24.65	–70.7(0.4)	0.78(0.01)
12/13	15.67	54.6(0.3)	0.62(0.01)
13/12	12.11	50.6(0.6)	0.77(0.02)
23[b]	11.50	18.8(0.1)	0.59(0.01)
31/32	5.66	–44.7(0.4)	0.65(0.02)
32/31	3.18	–43.5(0.5)	0.65(0.02)

[a] Values are established using data from the 5π-PULSE MAT experiment at B_0 = 16.4 T and ν_{MAS} = 2.3 kHz (Figure S12). Errors in the fit are provided in brackets for the anisotropy and asymmetry parameters (isotropic chemical shifts are taken directly from Table 1).

[b] Due to the small tensor anisotropy associated with this site, the shift tensor parameters extracted are not considered accurate.

Table S2. DFT-computed SCF energies for CSP-generated structures where $Z' = 1$

structure # (Fig. 8a)	structure name (CSP internal)	Z	E (eV)	E′ (eV/molec.)[a]	ΔE (kJ/molec.)[b]
1	1n_01_359_opt	4	-32132.663841	-8033.165960	9.269574
2	2_01_162_opt	2	-16065.654829	-8032.827415	41.934803
3	3_01_102_opt	2	-16065.328845	-8032.664423	57.661393
4	4_01_327_opt	4	-32130.743922	-8032.685981	55.581322
5	5_2_opt	2	-16065.561602	-8032.780801	46.432415
6	5_CSP_opt_07_60_opt	4	-32131.518932	-8032.879733	36.886755
7	5_final_opt	4	-32131.517875	-8032.879469	36.912244
8	5n_03_50_opt	4	-32131.497079	-8032.874270	37.413897
9	6_03_194_opt	4	-32131.011855	-8032.752964	49.118318
10	7n_02_92_opt	4	-32131.333950	-8032.833487	41.348846
11	8_01_249_opt	4	-32131.300708	-8032.825177	42.150704
12	9_01_383_opt	8	-64263.243487	-8032.905436	34.406758

13	10_opt_dimer_01_42_opt	2	-16065.564316	-8032.782158	46.301465
14	10n_01_65_opt	2	-16065.868005	-8032.934003	31.650456
15	12_01_409_opt	4	-32131.031744	-8032.757936	48.638561
16	13_05_109_opt	4	-32131.132608	-8032.783152	46.205560
17	14_01_160_opt	4	-32131.999936	-8032.999984	25.284106
18	15_01_219_opt	4	-32132.688855	-8033.172214	8.666181
19	16_01_143_opt	2	-16065.957768	-8032.978884	27.319974
20	17_01_57_opt	2	-16066.228230	-8033.114115	14.271972
21	18_01_35_opt	2	-16066.303154	-8033.151577	10.657367
22	18_2_01_211_opt	8	-64263.859937	-8032.982492	26.971842
23	18n_01_327_opt	8	-64263.901600	-8032.987700	26.469347
24	20_01_334_opt	4	-32132.451663	-8033.112916	14.387674
25	21_01_162_opt	4	-32131.115151	-8032.778788	46.626640
26	22_01_124_opt	2	-16066.250622	-8033.125311	13.191701
27	23_01_112_opt	4	-32131.707045	-8032.926761	32.349138
28	24_01_70_opt	2	-16065.495603	-8032.747802	49.616407
29	25_01_130_opt	4	-32131.521382	-8032.880345	36.827659
30	26_01_165_opt	8	-64264.294392	-8033.036799	21.731943
31	27_2_02_281_opt	8	-64261.034547	-8032.629318	61.048478
32	27n_02_489_opt	8	-64261.058895	-8032.632362	60.754832
33	28_01_164_opt	4	-32130.015579	-8032.503895	73.150220
34	29_01_143_opt	4	-32131.919226	-8032.979807	27.230969
35	30n_01_211_opt	4	-32131.433819	-8032.858455	38.939829
36	31_03_535_opt	8	-64262.613536	-8032.826692	42.004510
37	32_01_108_opt	8	-64264.831945	-8033.103993	15.248586
38	33_01_81_opt	4	-32131.443704	-8032.860926	38.701373
39	34_01_55_opt	4	-32131.364340	-8032.841085	40.615778
40	35_01_73_opt	2	-16066.007816	-8033.003908	24.905497
41	36_02_86_opt	4	-32131.854436	-8032.963609	28.793815
42	36_opt_02_258_opt	4	-32131.878250	-8032.969563	28.219378
43	37_3_01_91_opt	4	-32129.970758	-8032.492689	74.231391
44	37_twist_01_388_opt	4	-32130.281644	-8032.570411	66.732281
45	37n_01_348_opt	4	-32131.601030	-8032.900258	34.906401
46	38_01_10_opt	4	-32132.527008	-8033.131752	12.570233
47	39_01_54_opt	8	-64266.096248	-8033.262031	**0.000000**
48	40_01_33_opt	2	-16066.431597	-8033.215798	4.460855
49	41_01_73_opt	2	-16066.312235	-8033.156118	10.219270
50	42_01_42_opt	2	-16065.915678	-8032.957839	29.350524
51	43n_01_50_opt	2	-16066.159272	-8033.079636	17.598752
52	44_01_24_opt	4	-32131.855273	-8032.963818	28.773629
53	45_01_71_opt	4	-32131.398501	-8032.849625	39.791763
54	46_01_15_opt	2	-16065.688478	-8032.844239	40.311461
55	47_01_41_opt	4	-32130.091070	-8032.522768	71.329247

[a] Value is the reported energy (E) divided by the number of molecules per unit cell (i.e., $E' = E/Z$).
[b] Energy relative to the lowest structure (determined to be structure '47'/'39_01_54_opt').

Table S3. Normal distribution parameters for GIPAW DFT-calculated ^{13}C σ_{iso} and $\Delta\sigma$ parameters across the 55 CSP-generated structures ($Z' = 1$)[a]

label	$\overline{\sigma_{iso}}$ / ppm	$\sigma(\sigma_{iso})$ / ppm	$\kappa(\sigma_{iso})$ / ppm	$\overline{\Delta\sigma}$ / ppm	$\sigma(\Delta\sigma)$ / ppm	$\kappa(\Delta\sigma)$ / ppm
1	133.3	2.6	0.17	54.7	5.2	–0.43
3	119.5	2.4	0.73	49.4[b]	6.9	–0.45
4	101.7	3.5	0.36	64.0	7.6	–0.45
5	7.0	1.6	–1.03	133.0	3.7	–0.39
6	57.8	2.4	–1.36	165.2	3.7	1.01
7	38.0	1.7	–0.72	189.6	3.4	0.53
8	48.5	1.8	–0.20	177.1	4.9	0.56

9	36.6	2.1	0.31	175.8	4.6	0.65
10	37.4	1.6	–0.33	161.3	2.7	1.29
11	135.2	2.1	–1.09	76.9	3.3	1.16
12/13	156.9	2.6	0.50	–51.7	3.6	0.14
13/12	156.0	2.9	–1.10	–51.6	4.2	0.60
15	16.6	1.3	–0.55	128.8	3.6	–0.33
16	20.1	1.1	–0.54	–114.0	6.4	0.47
18	50.0	2.3	–0.11	–127.9	1.8	0.07
19	41.3	2.1	0.08	144.9[b]	2.3	0.05
21	24.9	1.3	0.31	133.9[b]	3.0	–0.86
22	39.0	1.6	0.20	167.2	2.7	–0.44
23	161.8	1.9	–0.47	23.4	2.5	–0.63
24	0.0	1.2	–0.18	–111.6	2.5	–0.18
25	53.1	1.9	0.40	159.4	6.5	–0.10
26	32.9	1.9	–0.40	170.7	4.0	0.50
27	45.7	2.3	0.00	165.0	6.2	–0.37
28	1.3	2.1	–0.11	129.1[b]	4.5	0.39
30	146.8	1.5	–0.65	74.6	2.9	–0.88
31/32	164.6	2.3	0.10	49.1[b]	3.5	0.47
32/31	164.1	2.7	0.35	49.4[b]	3.9	–0.01

[a] Site labels are as in Scheme 1 of the main paper. If desired, to convert the computed isotropic magnetic shielding values (σ_{iso}) into isotropic chemical shift values (δ_{iso}), the following may be used: δ_{iso} / ppm = 169.82 – σ_{iso} / ppm. Likewise, to convert computed magnetic shielding tensor anisotropy values ($\Delta\sigma$) into chemical shift tensor anisotropy values ($\Delta\delta$), the following may be used: $\Delta\delta$ / ppm = $-\Delta\sigma$ / ppm.
[b] Both positive and negative anisotropy values were calculated across the ensemble of structures. Thus we report here the average of the magnitudes for this parameter.

Table S4. DFT-computed SCF energies for CSP-generated structures where Z' = 2 (rigid)

structure # (Fig. 8b)	structure name (CSP internal)	Z	E (eV)	E′ (eV/molec.)[a]	ΔE (kJ/molec.)[b]
1	A-structure_01_27	8	-64264.956183	-8033.119523	13.750169
2	A-structure_01_29	8	-64265.446394	-8033.180799	7.837800
3	A-structure_01_30	8	-64265.412134	-8033.176517	8.251004
4	A-structure_01_31	8	-64264.570168	-8033.071271	18.405850
5	A-structure_01_32	8	-64264.402954	-8033.050369	20.422594
6	A-structure_01_33	8	-64264.516530	-8033.064566	19.052770
7	A-structure_01_34[c]	8	-32132.112551	-8033.028138	22.567631
8	A-structure_02_11	8	-64264.933141	-8033.116643	14.028073
9	B-structure_01_38	8	-64264.122607	-8033.015326	23.803813
10	B-structure_01_39	8	-64263.845888	-8032.980736	27.141283
11	B-structure_01_40	8	-64264.854116	-8033.106765	14.981185
12	B-structure_01_41	8	-64264.830022	-8033.103753	15.271780
13	B-structure_01_42	8	-64264.860993	-8033.107624	14.898245
14	B-structure_02_32	8	-64263.625311	-8032.953164	29.801632
15	B-structure_02_34	8	-64263.435518	-8032.929440	32.090700
16	B-structure_02_35[c]	8	-32131.821859	-8032.955465	29.579626
17	B-structure_03_10[c]	8	-32131.792862	-8032.948215	30.279097
18	B-structure_03_12[c]	8	-32131.821859	-8032.955465	29.579626
19	B-structure_03_13	8	-64264.086337	-8033.010792	24.241266
20	B-structure_03_14	8	-64263.806856	-8032.975857	27.612047
21	B-structure_03_15	8	-64264.847323	-8033.105915	15.063123
22	B-structure_03_16	8	-64263.417615	-8032.927202	32.306632
23	B-structure_03_19	8	-64263.426907	-8032.928363	32.194565
24	B-structure_03_22	8	-64264.063187	-8033.007898	24.520474
25	B-structure_03_25[c]	8	-32132.015416	-8033.003854	24.910696

[a] Reported energy (E) divided by the number of molecules per unit cell (i.e., E′ = E/Z).
[b] Energy relative to the lowest structure (i.e., '47'/'39_01_54_opt' from the Z′ = 1 CSP set).
[c] Unit cell symmetry was such that four molecules were required for the computation, rather than the full Z = 8.

Table S5. DFT-computed SCF energies for CSP-generated structures where Z′ = 2 (flexible)

structure # (Fig. 8b)	structure name (CSP internal)	Z	E (eV)	E′ (eV/molec.)[a]	ΔE (kJ/molec.)[b]
26	structure_01_14-castopt	8	-64264.178213	-8033.022277	23.133158
27	structure_01_18-castopt	8	-64264.263632	-8033.032954	22.102929
28	structure_01_20-castopt	8	-64264.194580	-8033.024322	22.935766
29	structure_01_21-castopt	8	-64264.676983	-8033.084623	17.117568
30	structure_01_22-castopt	8	-64263.640621	-8032.955078	29.616990
31	structure_01_25-castopt	8	-64264.157010	-8033.019626	23.388885
32	structure_01_30-castopt	8	-64263.690149	-8032.961269	29.019637
33	structure_05_40-castopt	8	-64264.209363	-8033.026170	22.757469
34	structure_05_50-castopt	8	-64263.768439	-8032.971055	28.075384
35	structure_05_54-castopt	8	-64263.729460	-8032.966182	28.545513

[a] Reported energy (E) divided by the number of molecules per unit cell (i.e., E′ = E/Z).
[b] Energy relative to the lowest structure, as before.

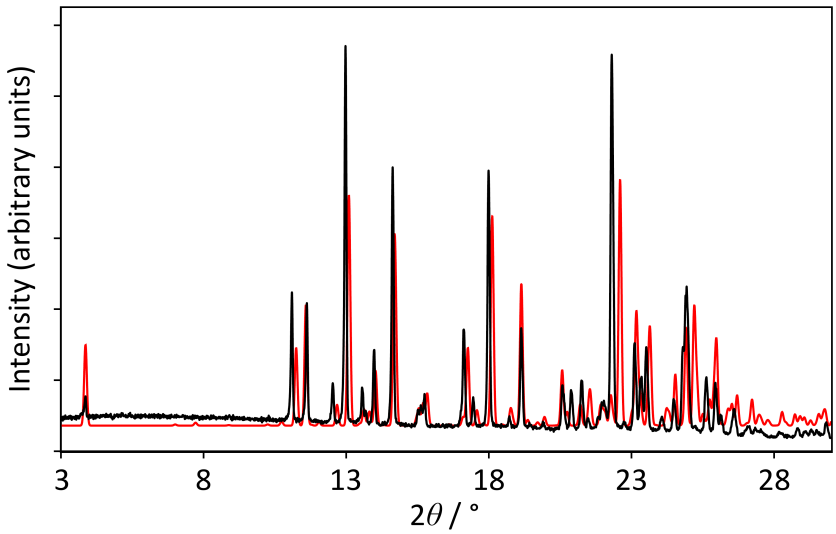

Figure S15. Simulated powder diffraction pattern (using the scXRD structure of **1** at 100 K) in red, and the experimental pXRD data acquired at room temperature, in black. The agreement is generally fairly good, yet clearly not optimal.

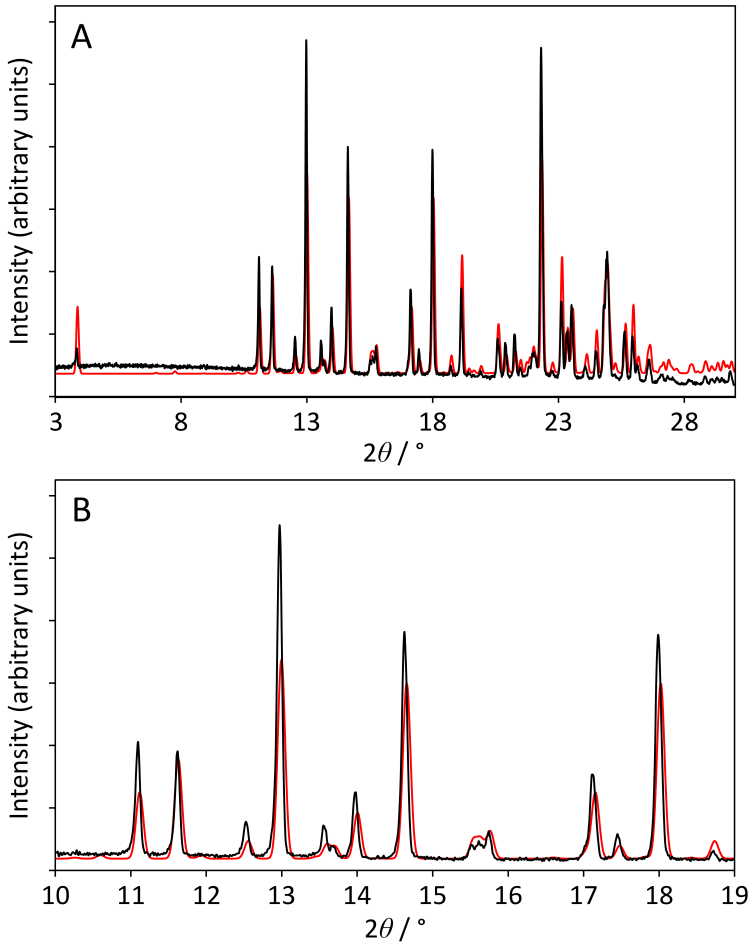

Figure S16. Comparison of simulated and experimental powder XRD patterns after adjusting the unit cell of the scXRD crystal structure determined at 100 K (original fractional atomic positions are retained from the diffraction structure of **1** at 100 K) such that it matched the unit cell measured for **1** at room temperature. In (**A**) very good agreement is seen over a range of reflections, while (**B**) shows the 2θ = 10 – 19° region only.

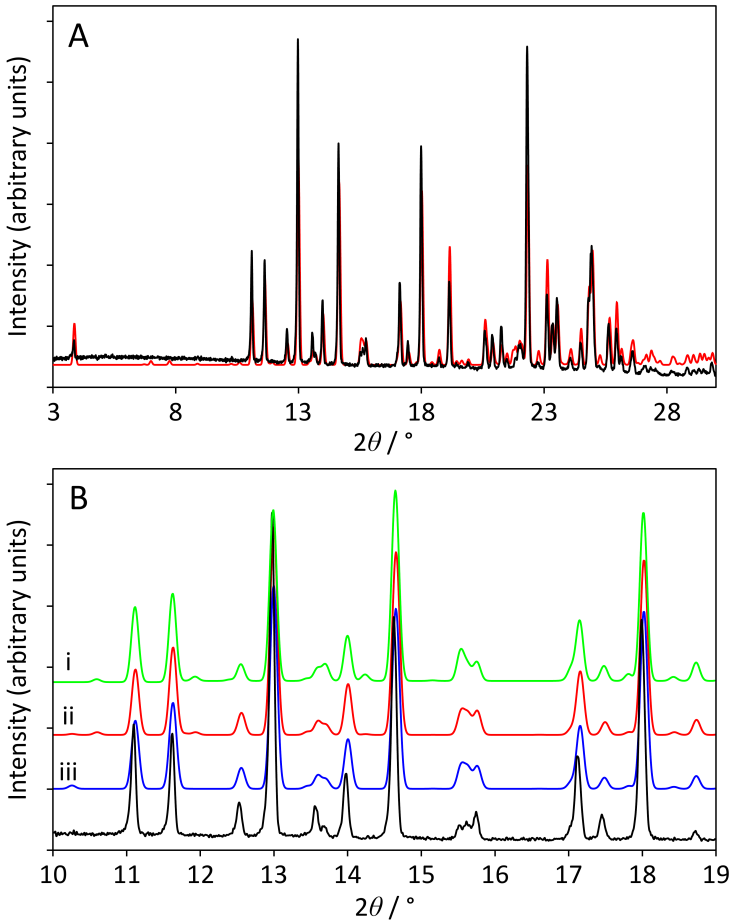

Figure S17. Comparison of the experimental powder XRD pattern, and those simulated after adjusting the unit cells of CSP-generated structures from the Z' = 2 set (original fractional atomic positions are retained for all CSP structures) such that they closely agreed with the unit cell measured for **1** at room temperature. In (**A**) very good agreement is seen over a range of reflections for CSP structure 2, while (**B**) shows the 2θ = 10 – 19° region for CSP structures 1 (i), 2 (ii), and 3 (iii).

Table S6. Direct space heavy atom RMSD values for leading CSP structures (Z' = 2, rigid)[a]

structure # (Fig. 8b)	space group	RMSD$_1$ / Å[b]	RMSD$_2$ / Å	RMSD$_4$ / Å	RMSD$_8$ / Å	RMSD$_{16}$ / Å
1	$P2_12_12_1$	0.044	0.056	0.116	0.256	—[c]
2	$P2_1/c$	0.044	0.056	0.111	0.166	0.166
3	$Pca2_1$	0.044	0.056	0.106	0.165	0.208

[a] Leading structures after considering all pXRD and SSNMR data.
[b] Subscript corresponds to the number of AZD7624 molecules which were attempted to be overlaid.
[c] Could not overlay all 16 molecules (15 out of 16 in this case).

References

1. U. Haeberlen, *Advances in Magnetic Resonance*, Academic Press, New York, 1976.
2. M. Mehring, *Principles of High Resolution NMR in Solids*, Springer-Verlag, Berlin, 2 edn., 1983.
3. H. W. Spiess, *NMR Basic Principles and Progress*, Springer-Verlag, Berlin, 1978.